# Simplified Lossless Analysis of Magnetoinductive Waveguides for Investigation of Impedance Termination on Power Nulling Characteristics

**Apisak Worapishet**
Mahanakorn Institute of Innovation (MII)
Mahanakorn University of Technology
140 Cheumsamphan Road, Kratumrai, Nongchok, Bangkok, Thailand 10530
Email: apisak@mut.ac.th

Manuscript received December 6, 2021
Revised December 24, 2021

**ABSTRACT**

***This work develops a simplified analysis of magnetoinductive (MI) waveguides under lossless and single load conditions. The formulation makes use of the relationship between the incident, reflected, and transmitted MI waves (MIWs) to enable explicit closed-form expressions of the current MIWs along the waveguide. By virtue of the analysis, investigation on the effect of the impedance termination on the power transfer characteristic of the MI waveguide is carried out, particularly under open, short and quadrature reactive impedance conditions. It is shown that although the quadrature impedance yields no current nulling at the center of each resonator cell, power transfer nulls still persist when the receiver is placed between cells that exhibit out-of-phase currents.***

***Keywords:*** *Wireless power transfer, magnetoinductive waveguide, LC resonator, power nulls.*

## 1. INTRODUCTION

Whereas wireless power charging to stationary devices becomes ubiquitous nowadays [1] - [3], emerging applications that require “dynamic” wireless power transfer (DWPT) to moving devices have started to gain traction. Among various DWPT methods [4] - [17], the magneto-inductive (MI) waveguides have shown promise to deliver wireless power over a long distance. However, its major drawback is the periodic power transfer nulls along its length, and various techniques have been introduced to mitigate the issue [14] - [17].

To study the power null characteristic, an analysis based on the propagation of magnetoinductive waves (MIWs) was elegantly presented in [14]. The analytical method relied on the relation between the effective terminating impedance and the reflectance, defined as the ratio between the reflected and incident MIWs, at a resonator cell of the waveguide. By referring all the impedances of the loaded cells back to the input cell through successive effective-impedance reflectance conversions, the current and power delivered into the line by the transmitting source were determined from the net effective terminating impedance ($Z_{eT}$) at the input cell. With subsequent calculations of the current and power delivered to the loads, analytical expressions describing power transfer efficiency were derived. Unlike the use of matrix inversion or continued fractions [15] - [17], the method offered a set of recursive equations for MI waveguides. Nevertheless, it is these successive impedance/reflectance conversions at every resonator cell from the termination to the input that make the analysis less explicit, with no concurrent MIW expressions throughout the waveguide.

Developed in this work is a more general analytical treatment of the MI waveguide that includes not only the reflectance but also the transmittance, defined as the ratio between the transmitted and incident MIWs. The inclusion of the transmittance enables more straight-forward and concurrent analysis, regardless of the number of receivers and terminations. Through simplification under single load and lossless conditions, this analysis results in explicit and concurrent MIW expressions, which may prove useful to providing more insight leading to a means to overcome to its perennial power null bottleneck.

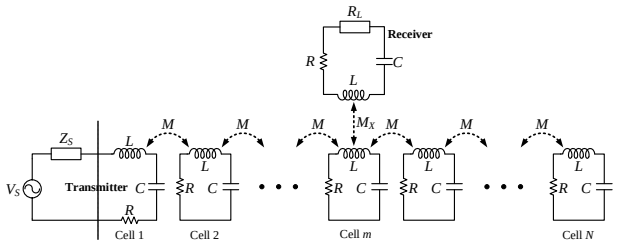


***Fig. 1*** *Equivalent circuit schematic of one-dimensional (1-D) MI waveguide with transmitter source $V_S$ and receiver cell with $R_L$.*

## 2. BASIC PROPERTIES OF MI WAVEGUIDES FOR WIRELESS POWER TRANSFER

A magnetoinductive or MI waveguide for wireless power transfer is typically formed by a chain of identical $LC$ resonator cells coupled via magnetic linkage between adjacent cells' coils. Fig. 1 shows an equivalent circuit schematic of a one-dimensional (1-D) MIW line with a transmitter or a power source at the first cell (cell 1), and a power extracting receiver coupled to the $m$th cell (cell $m$). Each of the resonator cells is modeled by a capacitance $C$ and an inductance $L$ with its associated loss $R$. The receiver is assumed to be an identical resonator cell loaded with a series resistance $R_L$. The magnetic coupling between cells along the waveguide is modeled by a mutual inductance $M$, where only a first-order coupling, $k = M/L$, between adjacent cells is assumed significant. The coupling to the receiver is modelled by the mutual inductance $M_X$. It should be noted that a co-planar MIW supports a backward propagating wave with a negative $k$ value [18] - [20]. For ease of description that follows, without loss of generality, a positive coupling factor $k$ with forward propagating wave is assumed unless stated otherwise.

In operation, the transmitter generates a MIW propagating along the cascaded cells of the waveguide. By locating the receiver at cell $m$, power can be coupled from the propagating MIW to the load $R_L$. Note that the receiver can be placed between cells so that both of the cells can couple power to the receiver. In wireless power transfer (WPT) applications, the operating frequency is typically in the vicinity of the cell's resonant frequency.

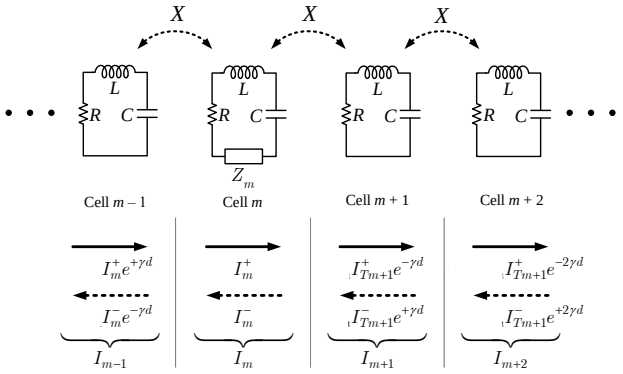


***Fig. 2*** *Section of 1-D MI waveguide comprising cell $m$ – 1 up to cell $m$ + 2.*

The wave propagation along the 1-D MIW line is generally expressed in terms of a circulating loop current at cell $n$, $I_n^{\pm} = I_0 e^{-n\gamma d} = I_0 e^{-n(\alpha d + j\beta d)}$, where $\gamma d = \alpha d + j\beta d$ denotes the propagation constant per cell, $\alpha d$ is the attenuation per cell, and $\beta d$ is the phase constant per cell.

With reference to Fig. 1, the MI waveguide is under a matched condition when the receiver is coupled to the last cell (cell $N$), and this yields a referred series load impedance $Z_0 = \omega_0 M e^{-\alpha d}$ at the resonant frequency $\omega_0$. In this case, the incident wave propagates toward cell $N$ with no reflection, delivering the maximum available power. When the receiver is coupled to cell $m (< N)$ before the last cell, however, a discontinuity is introduced even if it yields the same series impedance $Z_m = Z_0$. As a consequence, the MIW undergoes both reflection and transmission at the receiver cell $m$, as well as reflection at cell $N$, causing interference among the incident, transmitted and reflected waves. This in turn gives rise to a standing wave along the waveguide. This can adversely impact the power transfer efficiency and/or create power nulls, restricting its practical use for wireless power transfer.

## 3. MIW ANALYSIS USING REFLECTANCE /TRANSMITTANCE UNDER SINGLE LOAD AND LOSSLESS CONDITIONS

Let us consider a section of a 1-D MI waveguide comprising cell $m - 1$ up to cell $m + 2$ in Fig. 2. The effect of the receiver or termination at cell $m$ is modelled

by incorporating the series impedance $Z_m$ to study how the MIW is reflected and transmitted at the discontinuity. Under a single operating frequency at the resonant frequency $\omega_0 = 1/\sqrt{LC}$ and lossless conditions, we have $\alpha d = 0$, and the phase factor per cell $\beta d = \pi/2$. Thus, the wave propagation term $e^{\pm j\beta d} = e^{\pm j(\pi/2)} = \pm j$, and the matched receiver load is modelled by $Z_m = Z_0 = -jX = \omega_0 M$. By applying the Kirchhoff's voltage law, the recurrence equations in terms of the self-loop and coupled-loop currents $I_n$ governing the resonator cells $m$ and $m + 1$ are given, respectively, by

$$Z_m I_m + X\left(I_{m-1} + I_{m+1}\right) = 0 \tag{1a}$$

$$X\left(I_m + I_{m+2}\right) = 0 \tag{1b}$$

where $X = j\omega M$ is the mutual impedance between cells.

The steady-state current MIWs resulting from the discontinuity due to $Z_m$ are as depicted in Fig. 2. These include the incident wave at cell $m$ represented by the forward current $I_I$, the reflected wave at cell $m$ represented by the backward current $I_R$, the transmitted wave at cell $m + 1$ represented by the forward current $I_T e^{-j\pi/2} = -jI_T$, and the backward current $I'_R e^{+j\pi/2} = +jI'_R$ at cell $m + 1$, resulting from further reflections of the transmitted wave. Since the loop current in each cell is the sum of its total incident and reflected waves, we obtain the followings.

$$I_{m-1} = I_I e^{+j\pi/2} + I_R e^{-j\pi/2} = jI_I\left(1-\rho\right), \tag{2a}$$

$$I_m = I_I + I_R = I_I\left(1+\rho\right), \tag{2b}$$

$$I_{m+1} = I_T e^{-j\pi/2} + I'_R e^{+j\pi/2} = j\tau I_T\left(-1+\rho'\right), \tag{2c}$$

$$I_{m+2} = I_T e^{-j\pi} + I'_R e^{+j\pi} = -\tau I_T\left(1+\rho'\right). \tag{2d}$$

Note from the equations that the currents are also defined in terms of the reflectance $\rho = I_R/I_I$ and $\rho' = I'_R/I_T$, and the transmittance $\tau = I_T/I_I$. By substituting (2) into (1), it can be shown after some manipulation that the reflectance $\rho$ and the transmittance $\tau$ of the MI section in Fig. 2 are given by

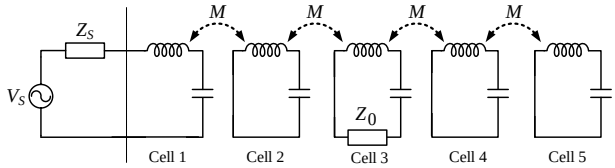


| | | | | | |
|---|---|---|---|---|---|
| $I_1^+ = +1$ | $I_2^+ = -j$ | $I_3^+ = -1$ | $I_4^+ = 0.5j$ | $I_5^+ = 0.5$ | $Z_5 = 0$ |
| $I_1^- = 0$ | $I_2^- = 0$ | $I_3^- = 0$ | $I_4^- = -0.5j$ | $I_5^- = 0.5$ | |
| $I_1 = +1$ | $I_2 = -j$ | $I_3 = -1$ | $I_4 = 0$ | $I_5 = +1$ | |

(a)

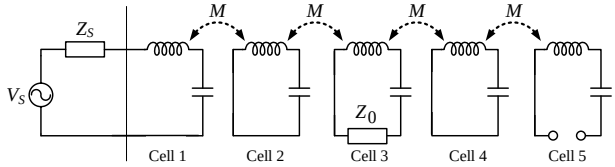


| | | | | | |
|---|---|---|---|---|---|
| $I_1^+ = +1$ | $I_2^+ = -j$ | $I_3^+ = -1$ | $I_4^+ = +j$ | $I_5^+ = +1$ | $Z_5 = \infty$ |
| $I_1^- = -1$ | $I_2^- = -j$ | $I_3^- = +1$ | $I_4^- = +j$ | $I_5^- = -1$ | |
| $I_1 = 0$ | $I_2 = -2j$ | $I_3 = 0$ | $I_4 = 2j$ | $I_5 = 0$ | |

(b)

***Fig. 3*** *Calculated propagating MIWs along the conventional MI waveguide at $N = 5$ and receiver at cell 3 under (a) $Z_N = 0$ and (b) $Z_N = \infty$.*

$$\rho = -\frac{\left(1-\rho'\right)Z_m - \rho' j2X}{\left(1-\rho'\right)Z_m + j2X}, \tag{3a}$$

$$\tau = \frac{1+\rho}{1+\rho'}. \tag{3b}$$

Note that (3a) is different from the reflectance equation derived in [14] due to the use of a different reference cell for the reflectance $\rho$. When $Z_m = 0$ and $\rho' = 0$ (no further reflection of the transmitted wave after cell $m$), we obtain $\rho = 0$ and $\tau = 1$ as expected. When cell $m$ is the last cell, we have the loop current $I_{m+1} = 0$, and thus $\rho' = -1$. Following this, the reflectance at cell $m = N$ in (5a) becomes

$$\rho_N = -\frac{Z_m + jX}{Z_m - jX} = -\frac{Z_m - Z_0}{Z_m + Z_0}. \tag{4}$$

Under a matched impedance $Z_m = Z_0 = -jX$, and the fact

that $\rho'_{m+1} = \rho_N e^{-j(N-m)\pi} = \rho_N(-1)^{N-m}$, the transmittance and reflectance at cell $m$ can thus be expressed in terms of the reflectance $\rho_N$ as

$$\rho_m = -\frac{1-\rho_N(-1)^{N-m}}{3+\rho_N(-1)^{N-m}}, \tag{5a}$$

$$\tau_{m+1} = \frac{2}{3+\rho_N(-1)^{N-m}}. \tag{5b}$$

Subsequently, the incident and reflected MIWs at cells 1 to $N$ of the lossless line with the single load at cell $m$ can be derived as

$$I_n^+ = \begin{cases} j^{-(n-1)}(-1)^{(n-1)}, & 1 \le n \le m \quad (6a) \\ \tau_{m+1} j^{-(n-1)}(-1)^{(n-1)}, & m+1 \le n \le N, \quad (6b) \end{cases}$$

$$I_n^- = \begin{cases} \rho_m I_n^+, & 1 \le n \le m \quad (7a) \\ \rho_N(-1)^{(N-n)} I_n^+, & m+1 \le n \le N. \quad (7b) \end{cases}$$

By utilizing the derived equations (3) to (7), the loop currents at any cell of a lossless MI waveguide with a matched load at cell $m$ can be determined without the need of successive impedance/reflectance conversions. Having finished the derivation, the characteristics of MIW-based WPT structures under different termination impedances can now be examined.

## 4. ANALYTICAL INVESTIGATION AND VERIFICATION

In this section, the derived equations in (3) to (7) are employed to investigate the conventional MI waveguides with open and short conditions as reported in [14]-[17]. In addition, the termination conditions under quadrature phase reactive impedance is analyzed. Comparisons with circuit simulation are also discussed.

### 4.1 CONVENTIONAL WPT WITH SHORT/OPEN TERMINATION

Let us consider the conventional lossless case with $Z_N = 0$ and $Z_N = \infty$ at $N = 5$ as a case example. By using (4), we have $\rho_N = +1$ and $-1$, respectively. By using (5), with the matched load at cell $m = 3$, we have $\rho_3 = 0$ and $\tau_4 = 0.5$ at $Z_N = 0$, and $\rho_3 = -1$ and $\tau_4 = +1$ at $Z_5 = \infty$. Subsequently, by using (6) and (7), the incident and reflected current MIWs can be shown in Fig. 3(a) for $Z_5 = 0$ and in Fig. 3(b) for $Z_5 = \infty$.

As noticed in the figures, the incident current wave from the source (cell 1) propagates with the associated phase constant per cell $\beta d = -\pi/2$ towards the last cell (cell 5) where it undergoes a total *in-phase* reflection under a short termination $Z_5 = 0$, and an *out-of-phase* reflection under an open termination $Z_5 = \infty$. While the reflected wave propagates back toward the source, it interferes with the incident wave creating a standing wave that exhibits both total summation and total cancellation or nulling of the loop currents. This is as indicated by $I_1$ to $I_5$ in Fig. 3(a) with opposite standing wave patterns under $Z_5 = 0$ and $Z_5 = \infty$. Consequently, power can be delivered to the load only when the receiver is located at any of the cells with no current nulling, in this case, at cell 3 for the short termination $Z_5 = 0$. It is important to note that the calculated total currents in the figures fully agree with circuit simulation.

### 4.2 QUADRATURE REACTIVE IMPEDANCE TERMINATION

Let us now consider a quadrature phase reflection by means of a reactive impedance termination at cell $N = 5$. By putting the reflectance $\rho_N = \pm j$ in (4), we obtain the terminating impedance $Z_N = \mathrm{m}X$, where $X$ is the mutual impedance between the cells. Under no receiver condition, by using (3) and (5), we have $\rho_3 = -j$ and $\tau_4 = +1$ at $Z_N = +X$, and $\rho_3 = +j$ and $\tau_4 = +1$ at $Z_N = -X$. As a result, by using (6) and (7), the incident and reflected currents can be shown in Fig. 4(a) for $Z_N = +X$ and in Fig. 4(b) for $Z_N = -X$.

Similarly, when the matched load is at cell $m = 3$, by using (5), we have $\rho_3 = -(0.2 + j0.4)$ and $\tau_4 = 0.6 + j0.2$ at $Z_N = +X$, and $\rho_3 = -(0.2 - j0.4)$ and $\tau_4 = 0.6 - j0.2$ at $Z_N = -X$. Following this, by using (6) and (7), the incident and reflected current MIWs can be shown in Fig. 5(a) for $Z_N = +X$ and in Fig. 5(b) for $Z_N = -X$. All the calculated currents in Fig. 4 and 5 completely agree with circuit simulation.

From Fig. 4 at no receiver, the resulting incident and reflected waves no longer exhibit equal magnitude but opposite phase characteristics at cell 1 up to the loaded cell (cell 3). As a results, there are no zero currents at any cell when the receiver is located at cell 3

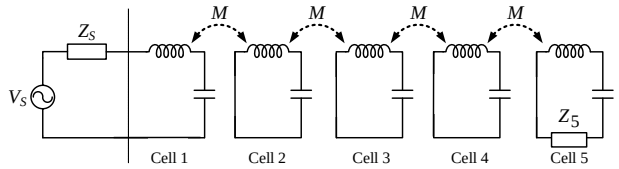


| | | | | | |
|---|---|---|---|---|---|
| $I_1^+ = +1$ | $I_2^+ = -j$ | $I_3^+ = -1$ | $I_4^+ = +j$ | $I_5^+ = +1$ | $Z_5 = +X$ |
| $I_1^- = -j$ | $I_2^- = +1$ | $I_3^- = +j$ | $I_4^- = -1$ | $I_5^- = -j$ | |
| $I_1 = 1-j$ | $I_2 = 1-j$ | $I_3 = -1+j$ | $I_4 = -1+j$ | $I_5 = 1-j$ | |

(a)

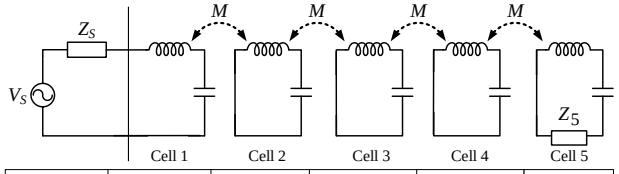


| | | | | | |
|---|---|---|---|---|---|
| $I_1^+ = +1$ | $I_2^+ = -j$ | $I_3^+ = -1$ | $I_4^+ = +j$ | $I_5^+ = +1$ | $Z_5 = -X$ |
| $I_1^- = +j$ | $I_2^- = -1$ | $I_3^- = -j$ | $I_4^- = +1$ | $I_5^- = +j$ | |
| $I_1 = 1+j$ | $I_2 = -1-j$ | $I_3 = -1-j$ | $I_4 = 1+j$ | $I_5 = 1+j$ | |

(b)

***Fig. 4*** *Current waves along the reactively terminated MI waveguide with no receiver at $N = 5$ under the termination impedance (a) $Z_N = +X$ and (b) $Z_N = -X$.*

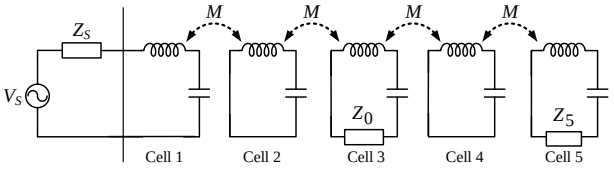


| | | | | | |
|---|---|---|---|---|---|
| $I_1^+ = +1$ | $I_2^+ = -j$ | $I_3^+ = -1$ | $I_4^+ =$ $-0.2+0.6j$ | $I_5^+ =$ $0.6+0.2j$ | $Z_5 = +X$ |
| $I_1^- =$ $-0.2-0.4j$ | $I_2^- =$ $0.4-0.2j$ | $I_3^- =$ $0.2+0.4j$ | $I_4^- =$ $-0.6-0.2j$ | $I_5^- =$ $0.2-0.6j$ | |
| $I_1 =$ $0.8-0.4j$ | $I_2 =$ $0.4-1.2j$ | $I_3 =$ $-0.8+0.4j$ | $I_4 =$ $-0.8+0.4j$ | $I_5 =$ $0.8-0.4j$ | |

(a)

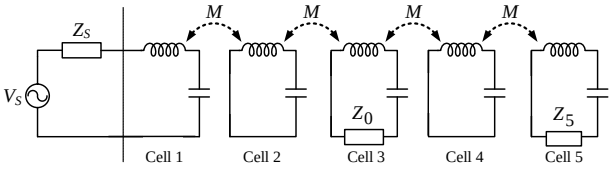


| | | | | | |
|---|---|---|---|---|---|
| $I_1^+ = +1$ | $I_2^+ = -j$ | $I_3^+ = -1$ | $I_4^+ =$ $0.2+0.6j$ | $I_5^+ =$ $0.6-0.2j$ | $Z_5 = -X$ |
| $I_1^- =$ $-0.2+0.4j$ | $I_2^- =$ $-0.4-0.2j$ | $I_3^- =$ $0.2-0.4j$ | $I_4^- =$ $0.6-0.2j$ | $I_5^- =$ $0.2+0.6j$ | |
| $I_1 =$ $0.8+0.4j$ | $I_2 =$ $-0.4-1.2j$ | $I_3 =$ $-0.8-0.4j$ | $I_4 =$ $0.8+0.4j$ | $I_5 =$ $0.8+0.4j$ | |

(b)

***Fig. 5*** *Current waves along the reactively terminated MI waveguide with receiver at cell 3 and $N = 5$ under the termination impedance (a) $Z_N = +X$ and (b) $Z_N = -X$.*

as shown in Fig. 5. At first glance, it seems that the quadrature termination could solve the power null issue. However, there is a case when the receiver is located in-between two resonator cells. Thus, if the adjacent cell currents are in opposite phase as in the case of Fig. 4(a) (cells 2 to 3, and cells 4 to 5), and Fig. 4(b) (cells 1 to 2, and cells 3 to 4), the power transfer will be cancelled out. Conseque-ntly, the quadrature termination still suffers from power transfer nulls.

## 5. CONCLUSION

A set of closed-form equations of magnetoinductive (MI) waveguides has been analyzed by using both the reflectance and transmittance of the MIW propagation. Under simplified lossless and single load conditions, a set of closed-form equations were developed, and subsequently employed to investigate power null characteristics of the waveguide under open, short and quadrature impedance terminations. It has been shown that the effect from power nulls cannot be mitigated by these terminations, particular when the receiver's mobility along the length of the entire waveguide is required. Nevertheless, the developed analysis with explicit current expressions should prove useful for future development of a means to eradicate the perennial power null issue.

## REFERENCES

[1] S. Y. Hui, ''Planar wireless charging technology for portable electronic products and qi,'' Proc. IEEE, vol. 101, no. 6, pp. 1290–1301, Jun. 2013.

[2] W. X. Zhong, X. Liu, and S. Y. R. Hui, ''A novel single-layer winding array and receiver coil structure for contactless battery charging systems with free-positioning and localized charging features,'' IEEE Trans. Ind. Electron., vol. 58, no. 9, pp. 4136–4144, Sep. 2011.

[3] D. McCormick, A. P. Hu, P. Nielsen, S. Malpas, and D. Budgett, "Powering implantable telemetry devices from localized magnetic fields," in Proc. 29th Annu. Int. Conf. IEEE Eng. Med. Biol. Soc., Aug. 2007, pp. 2331– 2335.

[4] Q. Xu, Z. Gao, H. Wang, J. He, Z. H. Mao, and M. Sun, "Batteries not included: A mat-based wireless power transfer system for implantable medical devices as a moving target," IEEE Microw. Mag., vol. 14, no. 2, pp. 63–72, Mar. 2013.

[5] S. A. Mirbozorgi, H. Bahrami, M. Sawan, and B. Gosselin, "A smart cage with uniform wireless power distribution in 3D for enabling long-term experiments with freely moving animals," IEEE Trans. Biomed. Circuits Syst., vol. 10, no. 2, pp. 424–434, Apr. 2016.

[6] C. J. Stevens, "Power transfer via metamaterials," Comput. Mater. Contin., vol. 33, no. 1, pp. 1–18, 2013.

[7] B. Wang, W. Yerazunis, and K. H. Teo, "Wireless power transfer: Metamaterials and array of coupled resonators," Proc. IEEE, vol. 101, no. 6, pp. 1359–1368, Jun. 2013.

[8] S. Y. R. Hui, W. Zhong, and C. K. Lee, "A critical review of recent progress in mid-range wireless power transfer," IEEE Trans. Power Electron., vol. 29, no. 9, pp. 4500–4511, Sep. 2014.

[9] C. C. Mi, G. Buja, S. Y. Choi, and C. T. Rim, ''Modern advances in wireless power transfer systems for roadway powered electric vehicles,'' IEEE Trans. Ind. Electron., vol. 63, no. 10, pp. 6533–6545, Oct. 2016.

[10] Y. Li, J. Hu, T. Lin, X. Li, F. Chen, Z. He, and R. Mai, ''A new coil structure and its optimization design with constant output voltage and constant output current for electric vehicle dynamic wireless charging,'' IEEE Trans. Ind. Informat., vol. 15, no. 9, pp. 5244–5256, Sep. 2019.

[11] K. Mori, H. Lim, S. Iguchi, K. Ishida, M. Takamiya, and T. Sakurai, "Positioning-free resonant wireless power transmission sheet with staggered repeater coil array (SRCA)," IEEE Antennas Wirel. Propag. Lett., vol. 11, pp. 1710–1713, 2012.

[12] S. A. Mirbozorgi, H. Bahrami, M. Sawan, and B. Gosselin, ''A smart multicoil inductively coupled array for wireless power transmission,'' IEEE Trans. Ind. Electron., vol. 61, no. 11, pp. 6061–6070, Nov. 2014.

[13] E. Waffenschmidt, "Homogeneous magnetic coup-ling for free positioning in an inductive wireless power system," IEEE J. Emerg. Sel. Topics Power Electron., vol. 3, no. 1, pp. 226–233, Mar. 2015.

[14] C. J. Stevens, "Magnetoinductive waves and wireless power transfer," *IEEE Trans Power Electron*., vol. 30, no. 11, pp. 6182–6190, Nov. 2015.

[15] G. Puccetti, C. J. Stevens, U. Reggiani, and L. Sandrolini, "Experimental and numerical investigation of termination impedance effects in wireless power transfer via metamaterial," Energies, vol. 8, no. 3, pp. 1882–1895, 2015.

[16] F. S. Sandoval, S. M. T. Delgado, A. Moazenzadeh, and U. Wallrabe, "Nulls-free wireless power transfer with straightforward control of magnetoinductive waves," *IEEE Trans. Microw. Theory Techn*., vol. 65, no. 4, pp. 1087–1093, Apr. 2017.

[17] F. S. Sandoval, S. M. T. Delgado, A. Moazenzadeh, and U. Wallrabe, "A 2-D magnetoinductive wave device for freer wireless power transfer," *IEEE Trans Power Electron*., vol. 34, no. 11, pp. 10433–10444, Nov. 2019.

[18] E. Shamonina, V. A. Kalinin, K. H. Ringhofer, and L. Solymar, "Magnetoinductive waves in one, two, and three dimensions," *J. Appl. Phys*.,vol. 92, no. 10, pp. 6252–6261, Nov. 2002.

[19] R. R. A. Syms, E. Shamonina, and L. Solymar, "Magneto-inductive waveguide devices," *IEE Proc.-Microw. Antennas Propag*., vol. 153, no. 2, pp. 111–121, Apr. 2006.

[20] L. Solymar, *Waves in Metamaterials*. London, U.K.: Oxford Univ. Press, 2009.

**Apisak Worapishet** received the B.Eng. degree (with first-class honors) from King Mongkut's Institute of Technology Ladkrabang, Bangkok, Thailand, in 1990, the M.Eng.Sc. degree from the University of New South Wales, Australia, in 1995, and the Ph.D. degree from Imperial College, London, U.K., in 2000, all in electrical engineering. Since 1990, he has been with Mahanakorn University of Technology, Bangkok, Thailand, where he currently serves as the Director of Mahanakorn Microelectronics Research Center (MMRC). He was the Editor-In-Chief of the ECTI Transactions on EEC from 2015 to 2019. Since 2016, he has served as the Associate Editor of IEEE Transactions on Circuits and Systems – I, Regular Papers.